Roles for Mitochondrial Complex I subunits in regulating synaptic transmission and growth

Bhagaban Mallik[1], C. Andrew Frank[1,2*]

[1]Department of Anatomy and Cell Biology, University of Iowa, USA, 52242

[2]Iowa Neuroscience Institute, University of Iowa Carver College of Medicine, Iowa City, IA, USA

*to whom correspondence should be addressed

andy-frank@uiowa.edu

Keywords: *Drosophila melanogaster*; synaptic homeostasis; neurotransmission; plasticity; mitochondria; Mitochondrial Complex I; *ND-20L*; HRP; NMJ; DLG

Abstract

To identify conserved components of synapse function that are also associated with human diseases, we conducted a genetic screen. We used the *Drosophila melanogaster* neuromuscular junction (NMJ) as a model. We employed RNA interference (RNAi) on selected targets and assayed synapse function by electrophysiology. We focused our screen on genetic factors known to be conserved from human neurological or muscle functions (321 total RNAi lines screened). Knockdown of a particular Mitochondrial Complex I (MCI) subunit gene (*ND-20L*) lowered levels of NMJ neurotransmission. Due to the severity of the phenotype, we studied MCI function further. Knockdown of core MCI subunits concurrently in neurons and muscle led to impaired neurotransmission. Further, pharmacology targeting MCI phenocopied the impaired neurotransmission phenotype. Finally, MCI subunit knockdowns led to profound cytological defects, including reduced NMJ growth and altered NMJ morphology. Mitochondria are essential for cellular bioenergetics and produce ATP through oxidative phosphorylation. Five multi-protein complexes achieve this task, and MCI is the largest. Impaired Mitochondrial Complex I subunits in humans are associated with disorders such as Parkinson's disease, Leigh syndrome, and cardiomyopathy. Together, our data present an analysis of Complex I in the context of synapse function and plasticity. We speculate that in the context of human MCI dysfunction, similar neuronal and synaptic defects could contribute to pathogenesis.

1. Introduction

Mitochondrial Complex I (MCI) is a multimeric enzyme with a molecular mass of about 1MDa (Hirst, 2013). It modulates the transfer of electrons from NADH to ubiquinone, facilitating ATP synthesis (Galkin et al., 2006; Galkin et al., 1999; Wikstrom, 1984). In humans, dysfunction of MCI activity can contribute to forms of neurodegeneration, and this is thought to be due to accumulation of excess reactive oxygen species (ROS) (Reviewed by (Breuer et al., 2013)). But on neuronal and synaptic levels, how exactly a buildup of ROS might manifest in disease phenotypes is unclear.

Structurally, Mitochondrial Complex I is comprised of 44 subunits in mammals; 42 of those are present in *Drosophila melanogaster* MCI, which is the focus of the present study (Garcia et al., 2017; Guerrero-Castillo et al., 2017). The 42 subunits of *Drosophila* MCI are comprised of 14 conserved subunits forming the catalytic core. The remaining 28 are termed accessory subunits (Garcia *et al.*, 2017) (Fig. 1A-B). Even though accessory subunits are not directly involved in catalysis, prior genetic and biochemical studies of MCI indicate that disruption of accessory subunits can produce high levels of reactive oxygen species (ROS), resulting in impaired MCI assembly and stability *in vivo* (Berger et al., 2008; Formosa et al., 2020; Guerrero-Castillo *et al.*, 2017; Stroud et al., 2016).

Mitochondrial Complex I subunits have been biochemically characterized from diverse species such as *Bos taurus* (Clason et al., 2010), *Yarrowia lipolytica* (Kashani-Poor et al., 2001; Radermacher et al., 2006), *Pichia pastoris* (Bridges et al., 2009), *Neurospora crassa* (Guenebaut et al., 1997; Leonard et al., 1987), *Drosophila melanogaster* (Garcia *et al.*, 2017), Humans (Murray et al., 2003) and rodents (Schilling et al., 2005). Electron microscopy approaches revealed that MCI has an L-shaped architecture, including arms that extend into the membrane and the periphery (Clason *et al.*, 2010; Guenebaut et al., 1998; Leonard *et al.*, 1987; Radermacher *et al.*, 2006). Subsequent X-ray crystallography analyses were performed in the entire mitochondrial complex from the *Y. lipolytica* at 6.3 Å resolution (Hunte et al., 2010).

Pharmacology in animal models has helped to elucidate some information about MCI activity and physiological consequences of its dysfunction. Two pharmacological agents that target MCI are rotenone and paraquat, which block the flow of electrons from NADH to

ubiquinone and trigger ROS formation in cells (Cocheme and Murphy, 2008; Degli Esposti, 1998; Fato et al., 2009). Studies in the fruit fly *Drosophila melanogaster* have assessed the effects of rotenone and paraquat on MCI *in vivo* physiology. In flies, paraquat impairs neuronal and mitochondrial function (Hosamani and Muralidhara, 2013). Similarly, delivering rotenone to flies triggers superoxide formation, leading to defects in locomotor ability (Leite et al., 2018). Antidotal pharmacology can abate these phenotypes. For example, eicosapentaenoic (EPA) and docosahexaenoic (DHA) omega-3 fatty acids reversed neurotoxic effects in flies induced by paraquat (de Oliveira Souza et al., 2019). Additionally, the sesquiterpene alcohol (-)-α-bisabolol (BISA) successfully reversed rotenone-induced locomotion and lethality phenotypes in flies (Leite *et al.*, 2018).

Genetic studies of MCI dysfunction in animals have shed light on possible physiological consequences of mutation of specific subunits (Mayr et al., 2015). One of these subunits, human NDUFS4, is required for MCI assembly, and misregulation of NDUFS4 has been linked with Leigh syndrome and cardiomyopathy (Fassone and Rahman, 2012). Modeling this deficiency in fruit flies, NDUFS4 depletion (Drosophila ND-18) leads to a state of progressive neurodegeneration, locomotor defects, and a shortened life span (Foriel et al., 2018). Additionally, among the mitochondrially-encoded MCI subunits, Drosophila ND2 loss-of-function mutants display behaviors reminiscent of human mitochondrial disease, including reduced life span and neurodegeneration (Burman et al., 2014). Recently, a genetic study disrupting mouse MCI specifically in dopaminergic neurons showed that loss of MCI alone was sufficient to induce progressive phenotypes reminiscent of Parkinson's Disease (Gonzalez-Rodriguez et al., 2021).

Despite the existence of animal genetic models – and despite the association of MCI dysfunction with human neurophysiological and neuromuscular disorders – extensive systematic functional analyses have not been performed to understand MCI roles on a subcellular level in neurons or synapses. Here, we report a small□scale electrophysiology-based RNA interference-based screen covering human neurological and muscle-related genes in *Drosophila* (321 lines). Our screen identified an MCI subunit line whose knockdown in the muscle and neuron led to aberrant neurotransmission. Follow-up electrophysiology showed that genetic depletion of other MCI subunit genes and pharmacology phenocopied this neurotransmission phenotype. On a

synapse level, we found that depletion of MCI subunits affected NMJ structural plasticity. Together, our data support a core role for MCI subunits in synaptic transmission and plasticity. Combined with prior studies, we argue that genetic modeling in fruit flies could be a useful way to understand the mechanisms of MCI subunits in synapse regulation. In turn, this establishes *Drosophila melanogaster* as a potential organism to further model MCI deficiency diseases.

2. Materials and methods

Drosophila husbandry

Drosophila melanogaster was cultured on a traditional cornmeal media containing molasses according to a recipe from the Bloomington *Drosophila* Stock Center (BDSC, Bloomington, IN). *Drosophila* husbandry was performed according to standard practices (James et al., 2019). For experiments, larvae were raised at 25°C or 29°C in humidity-controlled and light-controlled Percival DR-36VL incubators (Geneva Scientific).

Drosophila stocks

w^{1118} (Hazelrigg et al., 1984) was used as a non-transgenic wild-type stock. The *UAS-GluRIII[RNAi]* line was utilized to screen homeostatic candidate molecules as described previously (Brusich et al., 2015). The Gal4 drivers used simultaneously for the Pre+Post-Gal4 conditions were $elav^{C155}$-Gal4, *Sca*-Gal4, and *BG57*-Gal4. Many *UAS-RNAi* or genetic mutant lines were obtained from the Bloomington Drosophila Stock Center (Supplementary Table S3).

Immunohistochemistry

Wandering third instar larvae were dissected and fixed on a sylgard Petri plate in ice-cold Ca^{2+} HL-3 and fixed in 4% paraformaldehyde in PBS for 30 minutes or in Bouin's fixative for 2 minutes as described earlier (Raut et al., 2017). The larvae were washed with PBS containing 0.2% Triton X-100 (PBST) for 30 min, blocked for an hour with 5% normal goat serum in PBST, and incubated overnight in primary antibodies at 4°C followed by washes and incubation in secondary antibodies. Monoclonal antibodies such as anti-Dlg (4F3), anti-Synapsin (3C11) were obtained from the Developmental Studies Hybridoma Bank (University of Iowa, USA). All were used at 1:30 dilution. Fluorophore-coupled secondary antibodies Alexa Fluor 488, Alexa

Fluor 568 or Alexa Fluor 647 (Molecular Probes, Thermo Fisher Scientific) were used at 1:400 dilution. Alexa 488 or 647 and Rhodamine-conjugated anti-HRP were used at 1:800 and 1:600 dilutions, respectively (Jackson ImmunoResearch Laboratories, Inc.). The larval preparations were mounted in VECTASHIELD (Vector Laboratories, USA) and imaged with a laser scanning confocal microscope (LSM 710; Carl Zeiss). All the images were processed with Adobe Photoshop 7.0 (Adobe Systems, San Jose, CA).

Confocal imaging, quantification, and morphometric analysis

Samples were imaged using a 700 Carl Zeiss scanning confocal microscope equipped with 63×/1.4 NA oil immersion objective using separate channels with four laser lines (405, 488, 561, and 637 nm) at room temperature. The boutons were counted using anti-Synapsin co-stained with anti-Dlg on muscle 6/7 of A2 hemisegment, considering each Synapsin punctum to be a bouton. At least 8 NMJs were used for bouton number quantification. All genotypes were immunostained in the same tube with identical reagents for fluorescence quantifications of then mounted and imaged in the same session. Z-stacks were obtained using similar settings for all genotypes with z-axis spacing between 0.5-0.7 µm and optimized for detection without saturation of the signal. The Image J software (National Institutes of Health) analysis toolkit used maximum intensity projections for quantitative image analysis. Boutons from muscle 6/7 of A2 hemisegment from at least six NMJ synapses were used to quantify Image J software.

Statistical Analyses

Student's t-test for pairwise and One-way ANOVA with a Tukey's post-hoc test for multiple comparisons was used for statistical analysis (GraphPad Prism Software). Statistical tests are noted in the figure legends and supplementary table files and shown in graphs. The data are presented as mean±s.e.m. * $p < 0.05$, ** $p < 0.01$, *** $p < 0.001$.

Electrophysiology and pharmacology

All dissections and recordings were performed in a modified HL3 saline (Stewart et al., 1994) containing 70 mM NaCl, 5 mM KCl, 10 mM MgCl2, 10 mM NaHCO3, 115 mM sucrose, 4.2 mM trehalose, 5 mM HEPES, and 0.5 mM CaCl2 (unless otherwise noted), pH 7.2. Neuromuscular junction sharp electrode (electrode resistance between 20-30 MΩ) recordings were performed on muscles 6/7 of abdominal segments A2 and A3 in wandering third-instar larvae as described (James *et al.*, 2019). Larval NMJs recordings were performed on a Leica microscope in an HL3 buffer containing 10 mM Mg^{2+} and 0.5 mM Ca^{2+} concentrations using a 10x objective and acquired using an Axoclamp 900A amplifier, Digidata 1440A acquisition system, and pClamp 10.7 software (Molecular Devices). Electrophysiological sweeps were digitized at 10 kHz and filtered at 1 kHz. Data were analyzed using Clampfit (Molecular devices) and MiniAnalysis (Synaptosoft) software. Miniature excitatory post-synaptic potentials (mEPSPs) were recorded without any stimulation and motor axons were stimulated to elicit excitatory post-synaptic potentials (EPSPs). Average mEPSP, EPSP were determined for each muscle and quantal content was calculated by dividing average EPSP amplitude by average mEPSP amplitude. Muscle input resistance (R_{in}) and resting membrane potential (V_{rest}) were monitored during each experiment. Recordings were rejected if the V_{rest} was above -60 mV and R_{in} was less than 5 MΩ.

3. Results

An electrophysiology-based screen identifies Mitochondrial Complex I subunits in *Drosophila*

RNA interference (RNAi) is a powerful genetic approach. In *Drosophila*, RNAi screens have identified novel genes involved in diverse processes, such as nervous system development, eye development, and wound closure (Koizumi et al., 2007; Lesch et al., 2010; Pignoni et al., 1997; Raut *et al.*, 2017; Yamamoto et al., 2014). Prior reports indicate that many human diseases that affect muscle and nervous system health could have primary defects in synaptic function or plasticity (Hirth, 2010). However, the specific functional requirements remain unclear.

Our goal for this study was to survey homologs of selected human disease genes to test if they may also have conserved roles in synapse function or plasticity. We performed a targeted

RNAi-mediated reverse genetic screen in *Drosophila*. We picked 321 publicly available *UAS*-driven RNAi lines linked to human neurological and muscle-related disorders, and we knocked down the chosen target genes pan-neuronally and in muscles (Fig. 1A). Because RNAi-mediated knockdown can cause off-target effects or only partial depletion of gene function (Dietzl et al., 2007), we used multiple RNAi lines for genes, whenever possible.

Our main data collection assay was *Drosophila* neuromuscular junction (NMJ) electrophysiology. We recorded spontaneous miniature excitatory postsynaptic potentials (mEPSPs) and excitatory postsynaptic potentials (EPSPs). From these data we were able to assess for each gene knockdown: 1) baseline neurophysiology levels for quantal size, evoked potentials, and quantal content (see Methods); and 2) the maintenance of a form of synaptic plasticity, called presynaptic homeostatic potentiation (PHP). We assessed PHP via pre- and post-synaptic knockdown of an RNAi line plus knockdown of a glutamate receptor subunit gene (*GluRIII* RNAi), as we have shown previously, as a means of homeostatically challenging synapse function through decreased quantal size (Brusich *et al.*, 2015; James *et al.*, 2019).

Baseline control electrophysiology of the Gal4 driver lines alone yielded mEPSPs of 0.75 ± 0.03 mV, EPSPs of 37.67 ± 2.19 mV, and quantal content of 49.70 ± 1.71 (Fig. 2B, Table S1). Screened Gal4 + RNAi lines with average EPSP amplitudes ≤24 mV were classified as putative hits for this screen (Figure: 2B). These shortlisted RNAi lines were further tested for possible defects in PHP with concurrent knockdown of *GluRIII* RNAi.

The cumulative data revealed an intriguing phenotype for a line targeting *ND-20L*, an essential component of Mitochondrial Complex I (electron transport chain of mitochondria). Compared to the driver control alone, pre- + postsynaptic Gal4 drivers + *UAS-ND-20L[RNAi]* caused a significant defect in baseline evoked neurotransmission (Fig. 2B-D), no defect in quantal size (Fig. 2C-D), and a significant defect in calculated quantal content (QC, Fig. 2D). When presented the homeostatic challenge *UAS-GluRIII[RNAi]* genetic background, *ND-20L* knockdown by RNAi did decrease evoked neurotransmission (EPSP amplitude) significantly further than the non-challenged *ND-20L[RNAi]* control (Fig. 2C-D, Table S1). Yet there was nevertheless a slight homeostatic increase in QC (Fig. 2D). Together, our screen data suggest that Complex I subunits in *Drosophila* could regulate baseline synapse function by regulating the activity of the electron transport system. We tested this idea further.

Mitochondrial Complex I subunits in neurons and muscle regulate synapse function

ND-20L/NDUFS7 is a core MCI subunit. To assess whether synaptic transmission is altered after perturbation of other core MCI subunits, we recorded baseline NMJ neurotransmission after knocking down the subunits concurrently in neurons and muscle.

We acquired RNAi-based tools for all core subunits. In each case, the amplitudes of spontaneous miniature postsynaptic potentials (mEPSP) were not significantly altered in pre- + postsynaptic-depleted Complex I subunits (Fig 3A-S, Table S1). Nor did we find any notable change in mini frequency in pre- + postsynaptic knockdown of Complex I subunits (Table S1). However, for every case the amplitude of evoked postsynaptic potentials (EPSP) was numerically reduced after depleting Complex I, and quantal content (QC) was similarly reduced (Fig. 3A-U, Table S1). This numerical reduction in EPSP amplitude was statistically significant in 11/18 genetic lines we tested (Table S1). Of the 7 lines in which the EPSP reduction did not achieve statistical significance, 4 were mitochondrially-encoded (Table S1).

Because of the reduction of neurotransmission in many instances of MCI loss, we further checked if the NMJ could express PHP in the presence of *GluRIII* RNAi. As was the case with *ND-20L[RNAi]*, we found intact PHP signaling in most lines, as indicated by a significant increase in QC after *GluRIII* knockdown (Table S1). Together, our genetic data suggest that a majority of the core Complex I subunits in *Drosophila* regulate baseline synapse function. We decided to test this idea further by pharmacology.

Pharmocology phenocopies Mitochondrial Complex I subunit gene knockdown

Prior studies in *Drosophila* have targeted MCI via pharmacology. This has resulted in neurological and behavioral defects in adult flies reminiscent of human neurodegenerative conditions (Leite *et al.*, 2018). If it is the case that our genetic knockdown experiments are specific for MCI, then we should be able to phenocopy the NMJ electrophysiological defects with pharmacology. To target MCI, we used rotenone. Rotenone is an isoflavone derived from

plants, and it directly disrupts the electron transport chain of MCI and can result in an accumulation of reactive oxygen species (ROS) (Degli Esposti, 1998; Fato *et al.*, 2009).

We used several methods to deliver rotenone to the NMJ. We varied multiple parameters: drug concentation, exposure time, and delivery method. Larvae fed a low dose of rotenone (2 µM) for 48 hours showed no defect in evoked EPSP amplitude compared to carrier alone (5% DMSO, 48 hours, Figs. 4A-B, N). Likewise, freshly dissected NMJ preps acutely soaked in a high dose of rotenone (500 µM) showed little EPSP defect compared to carrier alone (5% DMSO, Figs. 4C-D, N).

However, larvae fed a high dose of rotenone (500 µM) for longer periods (72 hours or 7 hours) showed blunted EPSP amplitudes compared to carrier controls (Figs 4E-H, N). Additionally, larvae fed intermediate doses (25 µM or 50 µM) throughout life (approximately 120 hours from egg laying to third instar) also showed blunted EPSP amplitudes (Figs 4I-L, N).

Interestingly, not all of the delivery methods that caused a diminishment of EPSP amplitudes resulted in a decrease in quantal content (Figs 4M, O). This is because some delivery methods concurrently changed both quantal amplitude (Fig. 4M) and evoked amplitude (Fig. 4N). This may be because global application of a drug that impairs MCI could also have postsynaptic effects that govern sensitivity to individual vesicles of neurotransmitter.

Mitochondrial Complex I subunits regulate NMJ structural plasticity

We conducted NMJ staining experiments to assess if cytological phenotypes might accompany MCI loss. While Complex I subunits are expressed ubiquitously throughout the development, their roles in synapse development are largely unknown. To test this parameter, we knocked down some of the Complex I core subunits that we had previously analyzed electrophysiologically (using pre+post synaptic Gal4 drivers), but this time we analyzed the larval neuromuscular junction (NMJ) morphology. To visualize NMJ bouton morphology, and we co-stained with anti-Synapsin (a pre-synaptic marker) and anti-Discs Large (Dlg, a post-synaptic marker) (Benson and Voigt, 1995; Budnik et al., 1996).

Pre- + postsynaptic knockdown of Complex I subunits caused diminished NMJ structural development (Fig 5). For each subunit targeted, we observed diminished NMJ growth (Fig. 5A-F). This phenotype manifested in two different ways for different subunits: either as a decrease in total bouton number for animals reared at 25ºC (*mt: ND6[RNAi]*; *ND-51L2[RNAi]*) (Fig. 5F) or as a diminishment in bouton area (*ND-20L[RNAi]*) (Fig. 5G-I).

For the case of *ND-20L[RNAi]* the decreased bouton size was coupled with a collapsing postsynaptic density, as indicated by decreased amounts of Dlg (Fig. 5G-J). Together, these data indicate that Complex I subunits regulate NMJ growth and morphology in *Drosophila*. In this case, diminished NMJ development as a result of MCI loss (Fig. 5) correlates with diminished NMJ function (Figs. 2-3).

4. Discussion

Drosophila Mitochondrial Complex I subunits are highly conserved with their mammalian counterparts, potentially making *Drosophila* an ideal system to understand cellular MCI roles in diseases (Fig. 1). In this study, we provide a snapshot of synaptic phenotypes that result from MCI impairment in *Drosophila*. These initial studies should help us to dissect the function of MCI in nervous system physiology. Our aggregate data are consistent with the idea that normal MCI enzyme function is required to support normal levels of synaptic transmission (Figs. 2-4). Diminished synaptic neurotransmission may be related to blunted synapse development (Fig. 5).

Notably, our current study does not define the cell-specific roles that MCI is playing in pre- and postsynaptic compartments. In the context of human disease, genetic MCI loss is global and not tissue-specific. For future our studies, the genetic toolkit available for *Drosophila* means that it should be possible to define tissue specific roles of MCI, in presynaptic neurons, postsynaptic muscle, or in nearby tissue like glia.

Prior studies are consistent with synaptic functions of Complex I

Genetic dysfunction of MCI subunits produces superoxide in the mitochondrial matrix (Antonucci et al., 2019). Superoxide radicals can be converted into hydroxyl radicals that are

highly reactive and cause cellular damage. Pharmacological perturbation of Complex I with rotenone or paraquat stimulates ROS production both *in vivo* and *in vitro* (Cocheme and Murphy, 2008; Degli Esposti, 1998; Fato *et al.*, 2009). Relatedly, in adult *Drosophila*, Complex I inhibition by rotenone and paraquat triggers an acute response that is reminiscent of human mitochondrial disorder phenotypes (Hosamani and Muralidhara, 2013).

Although several genetic and biochemical studies have been performed to assess the efficacy of various compounds in suppressing rotenone and paraquat-induced toxicity in flies, little progress has been made to understand the precise consequences of Complex I dysfunction in nervous system physiology. Human mitochondrial disease-causing mutations have been identified in 33/44 MCI subunits (Mayr *et al.*, 2015). Mutation of *NDUFS4* causes Leigh syndrome and cardiomyopathy (Fassone and Rahman, 2012). In *Drosophila, dNDUFS4* depletion in neurons showed progressive neurodegeneration, shortened life span and locomotory defects, thus recapitulating patients with *NDUFS4* dysfunction (Foriel *et al.*, 2018). Additionally, ubiquitous knockdown of Drosophila *dNDUFS7* (*ND-20*) and *dNDUFV1* (*ND-51*) causes pupal eclosion defects and alternation in life span (Foriel et al., 2019). Many of these phenotypes are consistent with possible synapse dysfunction.

Recently, a *Drosophila* model of Complex I deficiency was created for mitochondrially encoded subunit ND2 (Burman *et al.*, 2014). The *dND-2* mutants showed hallmarks of mitochondrial diseases, which include progressive neurodegeneration, muscle degeneration and reduced life span (Burman *et al.*, 2014). Other reports have highlighted the role of neuron and glial cells in the context of neurodegeneration triggered by Complex I inhibition (Hegde et al., 2014). For instance, simultaneous disruption of *NDUFS1* in neurons and glia showed progressive neurodegeneration in flies, suggesting that both cell populations are essential in *Drosophila* (Hegde *et al.*, 2014). By contrast, depletion of *dNDUFS8* in glial cells did not affect longevity and locomotor ability in animals, while exhibiting significant neurodegeneration in the brain (Cabirol-Pol et al., 2018). A very similar phenotype was observed for *dNDUFS7B* where knockdown in neuron causes increased aggregation while exbiting no effect when depleted in glia (Li-Byarlay et al., 2014).

Possible Models: presynaptic release or postsynaptic ROS

Despite prior genetic and biochemical studies in the different model organisms, little information is known about the consequences of MCI dysfunction in nervous system at a single synapse level. At this point, we can propose a couple of different possibilities for impaired NMJ function and morphology. By one model, we can consider presynaptic compartment and synaptic vesicle fusion. Synaptic vesicle fusion is an energy-dependent process and depletion of Complex I subunits disrupts the transfer of electrons from NADH to ubiquinone. Hence, decreased proton motive force will reduce the amount of cellular ATP available for release.

By another model, disruption of Complex I in the muscle might produce elevated levels of reactive oxygen species intermediate (ROS), which are reactive and oxidizing. We speculate that ROS formation in the postsynaptic compartment might oxidize and disrupt postsynaptic structures such as Dlg (Fig. 5), Spectrin, and glutamate receptors that are crucial to maintaining a stable synaptic connection. The alteration of NMJ morphology could be a secondary consequence of the loss of postsynaptic structures, but it could also have a profound effect on synapse function. Our near-future studies on Complex I subunits will dissect distinct signaling mechanisms for Drosophila synapse regulation and function. In turn, studies downstream can test if these findings in our fruit fly model extend to vertebrate synaptic systems or mitochondrial disease models.

5. References

Antonucci, S., Mulvey, J.F., Burger, N., Di Sante, M., Hall, A.R., Hinchy, E.C., Caldwell, S.T., Gruszczyk, A.V., Deshwal, S., Hartley, R.C., et al. (2019). Selective mitochondrial superoxide generation in vivo is cardioprotective through hormesis. Free radical biology & medicine *134*, 678-687. 10.1016/j.freeradbiomed.2019.01.034.

Benson, T.E., and Voigt, H.F. (1995). Neuron labeling by extracellular delivery of horseradish peroxidase in vivo: a method for studying the local circuitry of projection and interneurons at physiologically characterized sites. J Neurosci Methods *57*, 81-91. 10.1016/0165-0270(94)00131-y.

Berger, I., Hershkovitz, E., Shaag, A., Edvardson, S., Saada, A., and Elpeleg, O. (2008). Mitochondrial complex I deficiency caused by a deleterious NDUFA11 mutation. Ann Neurol *63*, 405-408. 10.1002/ana.21332.

Breuer, M.E., Koopman, W.J., Koene, S., Nooteboom, M., Rodenburg, R.J., Willems, P.H., and Smeitink, J.A. (2013). The role of mitochondrial OXPHOS dysfunction in the development of neurologic diseases. Neurobiology of disease *51*, 27-34. 10.1016/j.nbd.2012.03.007.

Bridges, H.R., Grgic, L., Harbour, M.E., and Hirst, J. (2009). The respiratory complexes I from the mitochondria of two Pichia species. Biochem J *422*, 151-159. 10.1042/BJ20090492.

Brusich, D.J., Spring, A.M., and Frank, C.A. (2015). A single-cross, RNA interference-based genetic tool for examining the long-term maintenance of homeostatic plasticity. Frontiers in cellular neuroscience *9*, 107. 10.3389/fncel.2015.00107.

Budnik, V., Koh, Y.H., Guan, B., Hartmann, B., Hough, C., Woods, D., and Gorczyca, M. (1996). Regulation of synapse structure and function by the Drosophila tumor suppressor gene dlg. Neuron *17*, 627-640.

Burman, J.L., Itsara, L.S., Kayser, E.B., Suthammarak, W., Wang, A.M., Kaeberlein, M., Sedensky, M.M., Morgan, P.G., and Pallanck, L.J. (2014). A Drosophila model of mitochondrial disease caused by a complex I mutation that uncouples proton pumping from electron transfer. Dis Model Mech *7*, 1165-1174. 10.1242/dmm.015321.

Cabirol-Pol, M.J., Khalil, B., Rival, T., Faivre-Sarrailh, C., and Besson, M.T. (2018). Glial lipid droplets and neurodegeneration in a Drosophila model of complex I deficiency. Glia *66*, 874-888. 10.1002/glia.23290.

Clason, T., Ruiz, T., Schagger, H., Peng, G., Zickermann, V., Brandt, U., Michel, H., and Radermacher, M. (2010). The structure of eukaryotic and prokaryotic complex I. Journal of structural biology *169*, 81-88. 10.1016/j.jsb.2009.08.017.

Cocheme, H.M., and Murphy, M.P. (2008). Complex I is the major site of mitochondrial superoxide production by paraquat. J Biol Chem *283*, 1786-1798. 10.1074/jbc.M708597200.

de Oliveira Souza, A., Couto-Lima, C.A., Catalao, C.H.R., Santos-Junior, N.N., Dos Santos, J.F., da Rocha, M.J.A., and Alberici, L.C. (2019). Neuroprotective action of Eicosapentaenoic (EPA) and Docosahexaenoic (DHA) acids on Paraquat intoxication in Drosophila melanogaster. Neurotoxicology *70*, 154-160. 10.1016/j.neuro.2018.11.013.

Degli Esposti, M. (1998). Inhibitors of NADH-ubiquinone reductase: an overview. Biochimica et biophysica acta *1364*, 222-235. 10.1016/s0005-2728(98)00029-2.

Dietzl, G., Chen, D., Schnorrer, F., Su, K.C., Barinova, Y., Fellner, M., Gasser, B., Kinsey, K., Oppel, S., Scheiblauer, S., et al. (2007). A genome-wide transgenic RNAi library for conditional gene inactivation in Drosophila. Nature *448*, 151-156.

Fassone, E., and Rahman, S. (2012). Complex I deficiency: clinical features, biochemistry and molecular genetics. Journal of medical genetics *49*, 578-590. 10.1136/jmedgenet-2012-101159.

384 Fato, R., Bergamini, C., Bortolus, M., Maniero, A.L., Leoni, S., Ohnishi, T., and Lenaz, G.
385 (2009). Differential effects of mitochondrial Complex I inhibitors on production of reactive
386 oxygen species. Biochimica et biophysica acta *1787*, 384-392. 10.1016/j.bbabio.2008.11.003.

387 Foriel, S., Beyrath, J., Eidhof, I., Rodenburg, R.J., Schenck, A., and Smeitink, J.A.M. (2018).
388 Feeding difficulties, a key feature of the Drosophila NDUFS4 mitochondrial disease model. Dis
389 Model Mech *11*. 10.1242/dmm.032482.

390 Foriel, S., Renkema, G.H., Lasarzewski, Y., Berkhout, J., Rodenburg, R.J., Smeitink, J.A.M.,
391 Beyrath, J., and Schenck, A. (2019). A Drosophila Mitochondrial Complex I Deficiency
392 Phenotype Array. Front Genet *10*, 245. 10.3389/fgene.2019.00245.

393 Formosa, L.E., Muellner-Wong, L., Reljic, B., Sharpe, A.J., Jackson, T.D., Beilharz, T.H.,
394 Stojanovski, D., Lazarou, M., Stroud, D.A., and Ryan, M.T. (2020). Dissecting the Roles of
395 Mitochondrial Complex I Intermediate Assembly Complex Factors in the Biogenesis of
396 Complex I. Cell reports *31*, 107541. 10.1016/j.celrep.2020.107541.

397 Galkin, A., Drose, S., and Brandt, U. (2006). The proton pumping stoichiometry of purified
398 mitochondrial complex I reconstituted into proteoliposomes. Biochimica et biophysica acta *1757*,
399 1575-1581. 10.1016/j.bbabio.2006.10.001.

400 Galkin, A.S., Grivennikova, V.G., and Vinogradov, A.D. (1999). -->H+/2e- stoichiometry in
401 NADH-quinone reductase reactions catalyzed by bovine heart submitochondrial particles. FEBS
402 letters *451*, 157-161. 10.1016/s0014-5793(99)00575-x.

403 Garcia, C.J., Khajeh, J., Coulanges, E., Chen, E.I., and Owusu-Ansah, E. (2017). Regulation of
404 Mitochondrial Complex I Biogenesis in Drosophila Flight Muscles. Cell reports *20*, 264-278.
405 10.1016/j.celrep.2017.06.015.

406 Gonzalez-Rodriguez, P., Zampese, E., Stout, K.A., Guzman, J.N., Ilijic, E., Yang, B., Tkatch, T.,
407 Stavarache, M.A., Wokosin, D.L., Gao, L., et al. (2021). Disruption of mitochondrial complex I
408 induces progressive parkinsonism. Nature *599*, 650-656. 10.1038/s41586-021-04059-0.

409 Guarani, V., Paulo, J., Zhai, B., Huttlin, E.L., Gygi, S.P., and Harper, J.W. (2014).
410 TIMMDC1/C3orf1 functions as a membrane-embedded mitochondrial complex I assembly
411 factor through association with the MCIA complex. Mol Cell Biol *34*, 847-861.
412 10.1128/MCB.01551-13.

413 Guenebaut, V., Schlitt, A., Weiss, H., Leonard, K., and Friedrich, T. (1998). Consistent structure
414 between bacterial and mitochondrial NADH:ubiquinone oxidoreductase (complex I). Journal of
415 molecular biology *276*, 105-112. 10.1006/jmbi.1997.1518.

416 Guenebaut, V., Vincentelli, R., Mills, D., Weiss, H., and Leonard, K.R. (1997). Three-
417 dimensional structure of NADH-dehydrogenase from Neurospora crassa by electron microscopy
418 and conical tilt reconstruction. Journal of molecular biology *265*, 409-418.
419 10.1006/jmbi.1996.0753.

Guerrero-Castillo, S., Baertling, F., Kownatzki, D., Wessels, H.J., Arnold, S., Brandt, U., and Nijtmans, L. (2017). The Assembly Pathway of Mitochondrial Respiratory Chain Complex I. Cell metabolism *25*, 128-139. 10.1016/j.cmet.2016.09.002.

Hazelrigg, T., Levis, R., and Rubin, G.M. (1984). Transformation of white locus DNA in drosophila: dosage compensation, zeste interaction, and position effects. Cell *36*, 469-481.

Hegde, V.R., Vogel, R., and Feany, M.B. (2014). Glia are critical for the neuropathology of complex I deficiency in Drosophila. Human molecular genetics *23*, 4686-4692. 10.1093/hmg/ddu188.

Hirst, J. (2013). Mitochondrial complex I. Annu Rev Biochem *82*, 551-575. 10.1146/annurev-biochem-070511-103700.

Hirth, F. (2010). Drosophila melanogaster in the study of human neurodegeneration. CNS Neurol Disord Drug Targets *9*, 504-523. 10.2174/187152710791556104.

Hosamani, R., and Muralidhara (2013). Acute exposure of Drosophila melanogaster to paraquat causes oxidative stress and mitochondrial dysfunction. Arch Insect Biochem Physiol *83*, 25-40. 10.1002/arch.21094.

Hunte, C., Zickermann, V., and Brandt, U. (2010). Functional modules and structural basis of conformational coupling in mitochondrial complex I. Science *329*, 448-451. 10.1126/science.1191046.

James, T.D., Zwiefelhofer, D.J., and Frank, C.A. (2019). Maintenance of homeostatic plasticity at the Drosophila neuromuscular synapse requires continuous IP3-directed signaling. eLife *8*. 10.7554/eLife.39643.

Kashani-Poor, N., Kerscher, S., Zickermann, V., and Brandt, U. (2001). Efficient large scale purification of his-tagged proton translocating NADH:ubiquinone oxidoreductase (complex I) from the strictly aerobic yeast Yarrowia lipolytica. Biochimica et biophysica acta *1504*, 363-370. 10.1016/s0005-2728(00)00266-8.

Koizumi, K., Higashida, H., Yoo, S., Islam, M.S., Ivanov, A.I., Guo, V., Pozzi, P., Yu, S.H., Rovescalli, A.C., Tang, D., and Nirenberg, M. (2007). RNA interference screen to identify genes required for Drosophila embryonic nervous system development. Proc Natl Acad Sci U S A *104*, 5626-5631. 10.1073/pnas.0611687104.

Leite, G.O., Ecker, A., Seeger, R.L., Krum, B.N., Lugokenski, T.H., Fachinetto, R., Sudati, J.H., Barbosa, N.V., and Wagner, C. (2018). Protective effect of (-)-alpha-bisabolol on rotenone-induced toxicity in Drosophila melanogaster. Can J Physiol Pharmacol *96*, 359-365. 10.1139/cjpp-2017-0207.

Leonard, K., Haiker, H., and Weiss, H. (1987). Three-dimensional structure of NADH: ubiquinone reductase (complex I) from Neurospora mitochondria determined by electron microscopy of membrane crystals. Journal of molecular biology *194*, 277-286. 10.1016/0022-2836(87)90375-5.

457 Lesch, C., Jo, J., Wu, Y., Fish, G.S., and Galko, M.J. (2010). A targeted UAS-RNAi screen in
458 Drosophila larvae identifies wound closure genes regulating distinct cellular processes. Genetics
459 *186*, 943-957. 10.1534/genetics.110.121822.

460 Li-Byarlay, H., Rittschof, C.C., Massey, J.H., Pittendrigh, B.R., and Robinson, G.E. (2014).
461 Socially responsive effects of brain oxidative metabolism on aggression. Proc Natl Acad Sci U S
462 A *111*, 12533-12537. 10.1073/pnas.1412306111.

463 Mayr, J.A., Haack, T.B., Freisinger, P., Karall, D., Makowski, C., Koch, J., Feichtinger, R.G.,
464 Zimmermann, F.A., Rolinski, B., Ahting, U., et al. (2015). Spectrum of combined respiratory
465 chain defects. J Inherit Metab Dis *38*, 629-640. 10.1007/s10545-015-9831-y.

466 Murray, J., Zhang, B., Taylor, S.W., Oglesbee, D., Fahy, E., Marusich, M.F., Ghosh, S.S., and
467 Capaldi, R.A. (2003). The subunit composition of the human NADH dehydrogenase obtained by
468 rapid one-step immunopurification. J Biol Chem *278*, 13619-13622. 10.1074/jbc.C300064200.

469 Pignoni, F., Hu, B., and Zipursky, S.L. (1997). Identification of genes required for Drosophila
470 eye development using a phenotypic enhancer-trap. Proc Natl Acad Sci U S A *94*, 9220-9225.
471 10.1073/pnas.94.17.9220.

472 Radermacher, M., Ruiz, T., Clason, T., Benjamin, S., Brandt, U., and Zickermann, V. (2006).
473 The three-dimensional structure of complex I from Yarrowia lipolytica: a highly dynamic
474 enzyme. Journal of structural biology *154*, 269-279. 10.1016/j.jsb.2006.02.011.

475 Raut, S., Mallik, B., Parichha, A., Amrutha, V., Sahi, C., and Kumar, V. (2017). RNAi-Mediated
476 Reverse Genetic Screen Identified Drosophila Chaperones Regulating Eye and Neuromuscular
477 Junction Morphology. G3 (Bethesda) *7*, 2023-2038. 10.1534/g3.117.041632.

478 Schilling, B., Bharath, M.M.S., Row, R.H., Murray, J., Cusack, M.P., Capaldi, R.A., Freed, C.R.,
479 Prasad, K.N., Andersen, J.K., and Gibson, B.W. (2005). Rapid purification and mass
480 spectrometric characterization of mitochondrial NADH dehydrogenase (Complex I) from rodent
481 brain and a dopaminergic neuronal cell line. Mol Cell Proteomics *4*, 84-96.
482 10.1074/mcp.M400143-MCP200.

483 Stewart, B.A., Atwood, H.L., Renger, J.J., Wang, J., and Wu, C.F. (1994). Improved stability of
484 Drosophila larval neuromuscular preparations in haemolymph-like physiological solutions. J
485 Comp Physiol A *175*, 179-191. 10.1007/BF00215114.

486 Stroud, D.A., Surgenor, E.E., Formosa, L.E., Reljic, B., Frazier, A.E., Dibley, M.G., Osellame,
487 L.D., Stait, T., Beilharz, T.H., Thorburn, D.R., et al. (2016). Accessory subunits are integral for
488 assembly and function of human mitochondrial complex I. Nature *538*, 123-126.
489 10.1038/nature19754.

490 Wikstrom, M. (1984). Two protons are pumped from the mitochondrial matrix per electron
491 transferred between NADH and ubiquinone. FEBS letters *169*, 300-304. 10.1016/0014-
492 5793(84)80338-5.

493 Yamamoto, S., Jaiswal, M., Charng, W.L., Gambin, T., Karaca, E., Mirzaa, G., Wiszniewski,
494 W., Sandoval, H., Haelterman, N.A., Xiong, B., et al. (2014). A drosophila genetic resource of
495 mutants to study mechanisms underlying human genetic diseases. Cell *159*, 200-214.
496 10.1016/j.cell.2014.09.002.

497

6. Figure Legends

Figure 1: Organization and classification of *Drosophila* Mitochondrial Complex I (Cl) subunits

(A) Schematic showing how Mitochondrial Complex I (MCI) is organized into three distinct classes of subunits (Nuclear-encoded core: 7 subunits, mitochondrial-encoded: 7 subunits and nuclear-encoded accessory: 28 subunits). (B) Schematic representation of how the 42 different subunits of *Drosophila* MCI are arranged to produce the L-shaped topology; adapted from (Guarani et al., 2014). NDUFS7/S7 (*ND-20L*) is labeled in red.

Figure 2. An RNAi screen to identify genes involved in homeostatic synaptic plasticity for human neurological and muscle-related disorders in *Drosophila*.

(A) Crossing scheme for screen. Pre+Post-Gal4; *GluRIII*[RNAi] × *UAS-yfg*[RNAi] (*yfg*, "your favorite gene"). For UAS-RNAi lines on chromosomes II or III, male progeny were examined by electrophysiology because dosage compensated *elaV(C155)-Gal4/Y* male progeny should have a higher dose of pre-synaptic Gal4 than *elaV(C155)*-Gal4/+ female siblings. (B) Screen results are highlighted with red and blue bars in the histogram. EPSP ≤ 24 mV and ≥ 28 mV were considered as hits and normal phenotypes, respectively. (C) Representative electrophysiological traces for indicated genotypes in the presence and absence of *GluRIII* RNAi. Scale bars for EPSPs (mEPSPs) are x = 50 ms (1000 ms) and y = 10 mV (1 mV). (D) Quantification showing mEPSP, EPSPs amplitude and quantal content in pre+post-Gal4(mEPSP: 0.93 ± 0.05, EPSP: 38.99 ± 2.02, QC: 42.20 ± 2.65), pre+post-*GluRIII* RNAi (mEPSP: 0.49 ± 0.03, EPSP: 35.08 ± 0.82, QC: 73.82 ± 6.52), pre+post *ND-20L* RNAi (mEPSP: 0.80 ± 0.03, EPSP: 27.44 ± 0.70, QC: 34.44 ± 1.34) and pre+post *ND-20L+GluRIII* RNAi (mEPSP: 0.44 ± 0.05, EPSP: 19.55 ± 0.68, QC: 48.18 ± 6.95). The data for pre+post *ND-20L* RNAi and pre+post *ND-20L+GluRIII* RNAi are also represented in the supplemental Table S1. Statistical analysis based on one-way

ANOVA with Tukey's post-hoc test. Error bars represent mean±s.e.m. * $p < 0.05$, ** $p < 0.01$, *** $p < 0.001$.

Figure 3: Core complex I subunits regulate neurotransmission (A-R) Representative traces for pre+post-Gal4 driven Mitochondrial Complex I subunits in the presence and absence of *GluRIII* RNAi. Scale bars for EPSPs (mEPSPs) are x = 50 ms (1000 ms) and y = 10 mV (1 mV). (S-U) Histogram showing average mEPSP, EPSPs amplitude and quantal content in Pre+post-Gal4 control, Pre+post-Gal4 driven *GluRIII* RNAi, Pre+post-Gal4 driven MCI subunits and Pre+post-Gal4 driven *GluRIII* RNAi and MCI RNAi core subunits in the indicated genotypes. At least 8 NMJ recordings of each genotype were used for quantification. Pre- and postsynaptic RNAi corresponding to nuclear and mitochondrial encoded MCI subunits were analyzed for EPSPs through electrophysiological recordings. *p*-values for EPSPs are indicated in Table S1. Statistical analysis based on Student's t-test for pairwise comparisons (in determining PHP for a specific genotype), or one-way ANOVA followed by post-hoc Tukey's multiple comparisons. Error bars represent mean±s.e.m. * $p < 0.05$, ** $p < 0.01$, *** $p < 0.001$.

Figure 4: Rotenone diminishes neurotransmission at the NMJ (A-L) Representative traces for third instar wild-type larvae treated or fed with DMSO and rotenone at various concentrations as indicated above. Scale bars for EPSPs (mEPSPs) are x = 50 ms (1000 ms) and y = 10 mV (1 mV). (M-O) Histogram showing average mEPSP, EPSPs amplitude and quantal content of larvae treated with DMSO and rotenone in the indicated conditions. Note that larvae treated or fed a high dose of rotenone showed decreased EPSP amplitudes compared to carrier controls. At least 8 NMJs recordings of each genotype were used for quantification. *p*-values for EPSPs are indicated in Table S2. Statistical analysis based on Student's t-test for pairwise comparison. Error bars represent mean±s.e.m.

Figure 5: *Drosophila* Mitochondrial Complex I subunits are required for normal neuromuscular junction (NMJ) morphology.

(A-E) Representative confocal images of NMJ synapses at muscle 6/7 of (A) Pre+post-Gal4 control (105.0 ± 6.38), Pre+post-Gal4 driven (B) *ND-20L* RNAi (108.9 ± 8.01), (C) *mt: ND6* RNAi (72.75 ± 4.77), (D) *ND-51L2* RNAi (73.88 ± 4.50) and (E) *ND-51* RNAi (64.63 ± 7.46) flies double immunolabeled with Dlg (magenta) and synapsin (green) antibodies. The NMJ morphological defects were observed in the indicated genotypes. Scale bar: 10 µm. (F) Histograms showing the average total number of boutons at muscle 6/7 of A2 hemisegment in Pre+post-Gal4 control (105.0 ± 6.38), Pre+post-Gal4 driven *ND-20L* RNAi (108.9 ± 8.01), *mt: ND6* RNAi (72.75 ± 4.77), *ND-51L2* RNAi (73.88 ± 4.50), control (75.86 ± 8.57) and *ND-51* RNAi (64.63 ± 7.46) larvae. (G-H) Confocal images of boutons at third instar larval NMJ synapse in (G) Pre+post-Gal4 control and (H) Pre+post-Gal4 driven *ND-20L* RNAi double immunolabeled with Dlg (magenta) and HRP (green) antibodies. Note that the gross morphology of SSR and the immunoreactivity of Dlg were reduced in *ND-20L* RNAi compared to control. (I-J) Histograms showing average bouton area (I) relative Dlg area (J) in μm^2 of Pre+post-Gal4 control (bouton area: 11.49 ± 0.88, relative Dlg area: 8.93 ± 0.65), Pre+post-Gal4 driven *ND-20L* RNAi bouton area: (6.12 ± 0.34, relative Dlg area: 4.74 ± 0.29) larvae. Scale bar represents 10 µm. Statistical analysis based on Student's t-test for pairwise comparison and one-way ANOVA with Tukey's post-hoc test for multiple comparisons. Error bars represent mean±s.e.m. * $p < 0.05$, ** $p < 0.01$, *** $p < 0.001$.

7. Conflicts of interest

The authors declare that the research was conducted in the absence of any commercial or financial relationships that could be construed as a potential conflict of interest.

8. Author contributions

B.M. and C.A.F. designed the research; B.M. performed the research; B.M. and C.A.F. analyzed the data; B.M. and C.A.F. wrote the paper.

9. Funding

This work was supported by a grant from the National Institutes of Health/NINDS (R01NS085164) to C.A.F. B.M. was supported in part by this grant.

10. Acknowledgments

We acknowledge the Developmental Studies Hybridoma Bank (Iowa, USA) for antibodies used in this study and the Bloomington Drosophila Stock Center for fly stocks. We thank Frank lab members for their helpful comments and discussions in this study. For research in progress discussions, we thank members of the laboratories of Drs. Tina Tootle, Toshihiro Kitamoto, Pamela Geyer, and Lori Wallrath; we also thank faculty from the Department of Anatomy and Cell Biology at the University of Iowa for weekly workshop discussions.

11. Supplementary Material

Please see Supplementary Tables S1-S3. Table S1 shows raw electrophysiology data for Mitochondrial Complex I loss-of-function conditions. Table S2 shows raw electrophysiology data for rotenone application. Table S3 details *Drosophila* stocks and antibodies used.

12. Data Availability Statement

The raw data supporting the conclusions in this article will be made available by the authors, without undue reservation.

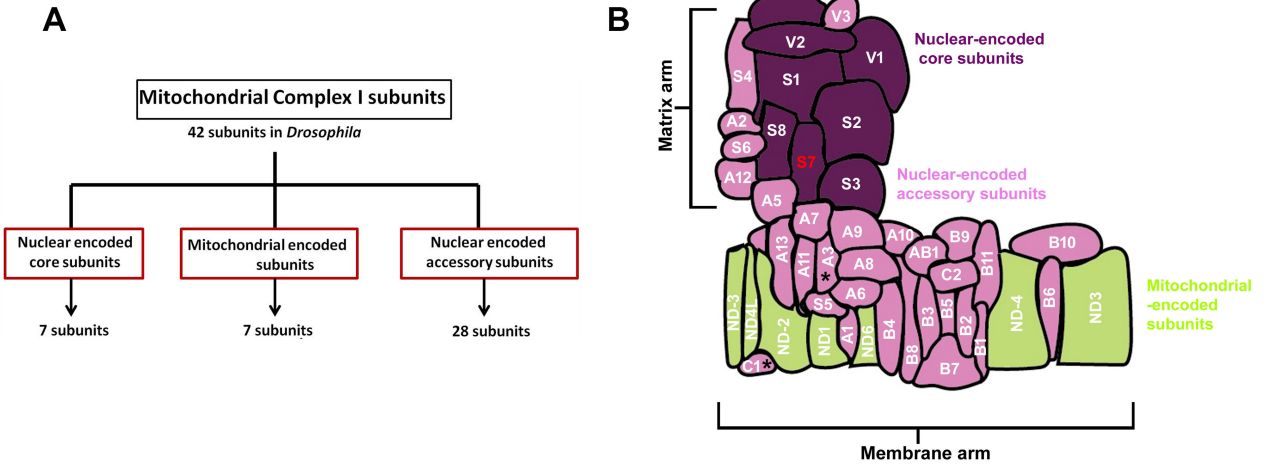
A
Mitochondrial Complex I subunits
42 subunits in Drosophila
Nuclear encoded core subunits
Mitochondrial encoded subunits
Nuclear encoded accessory subunits
7 subunits
7 subunits
28 subunits
B
Matrix arm
Nuclear-encoded core subunits
Nuclear-encoded accessory subunits
Mitochondrial -encoded subunits
Membrane arm
* No Drosophila ortholog identified
Adapted from Guarani et.al., 2014

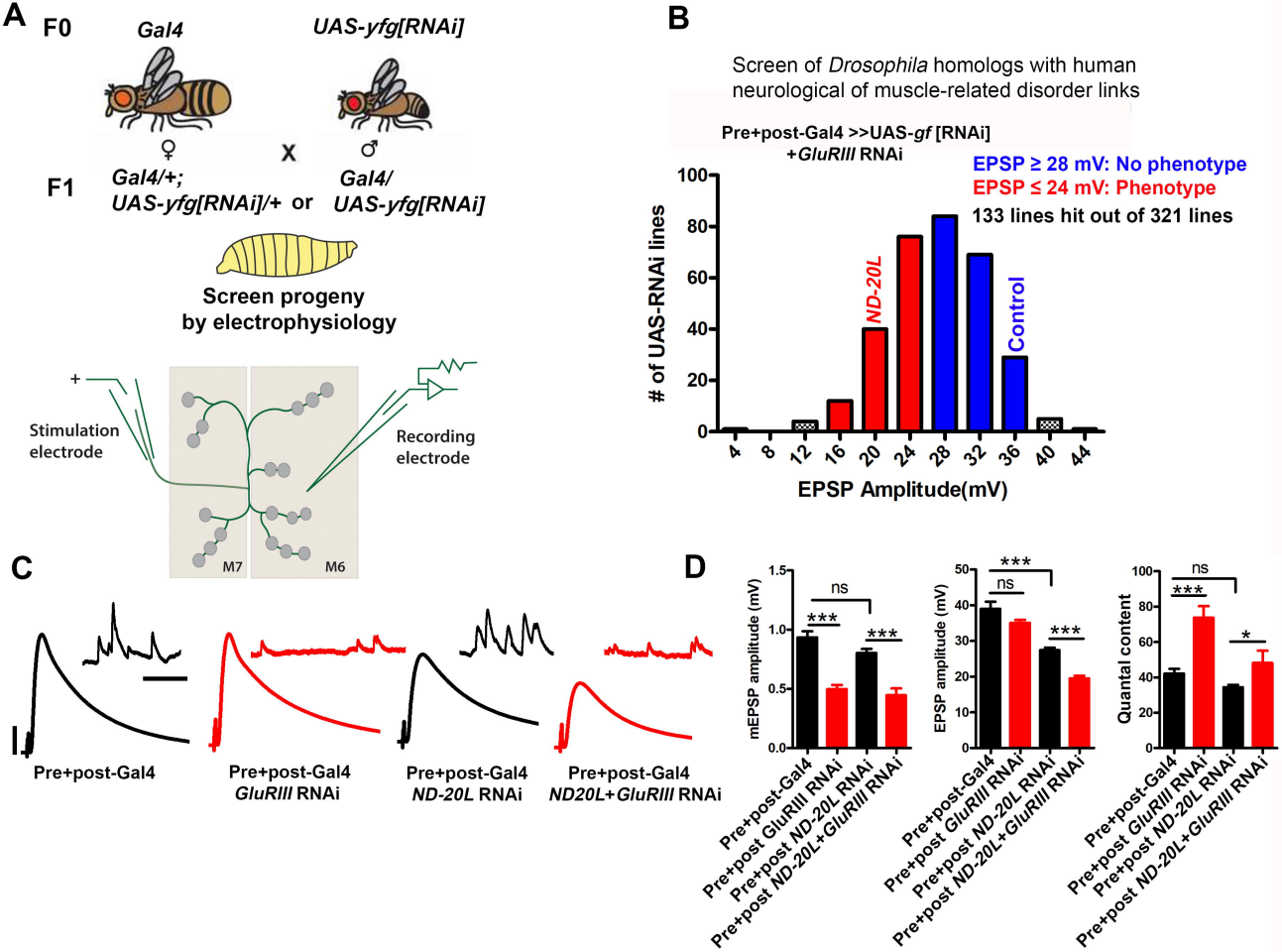
A
F0
Gal4
UAS-yfg[RNAi]
♀
X
♂
F1
Gal4/+;
UAS-yfg[RNAi]/+ or
Gal4/
UAS-yfg[RNAi]
Screen progeny
by electrophysiology
+
Stimulation
electrode
Recording
electrode
M7
M6
B
Screen of Drosophila homologs with human
neurological of muscle-related disorder links
Pre+post-Gal4 >>UAS-gf [RNAi]
+GluRIII RNAi
EPSP ≥ 28 mV: No phenotype
EPSP ≤ 24 mV: Phenotype
133 lines hit out of 321 lines
# of UAS-RNAi lines
ND-20L
Control
EPSP Amplitude(mV)
C
Pre+post-Gal4
Pre+post-Gal4
GluRIII RNAi
Pre+post-Gal4
ND-20L RNAi
Pre+post-Gal4
ND20L+GluRIII RNAi
D
mEPSP amplitude (mV)
EPSP amplitude (mV)
Quantal content
ns
***
*
Pre+post-Gal4
Pre+post GluRIII RNAi
Pre+post ND-20L RNAi
Pre+post ND-20L+GluRIII RNAi

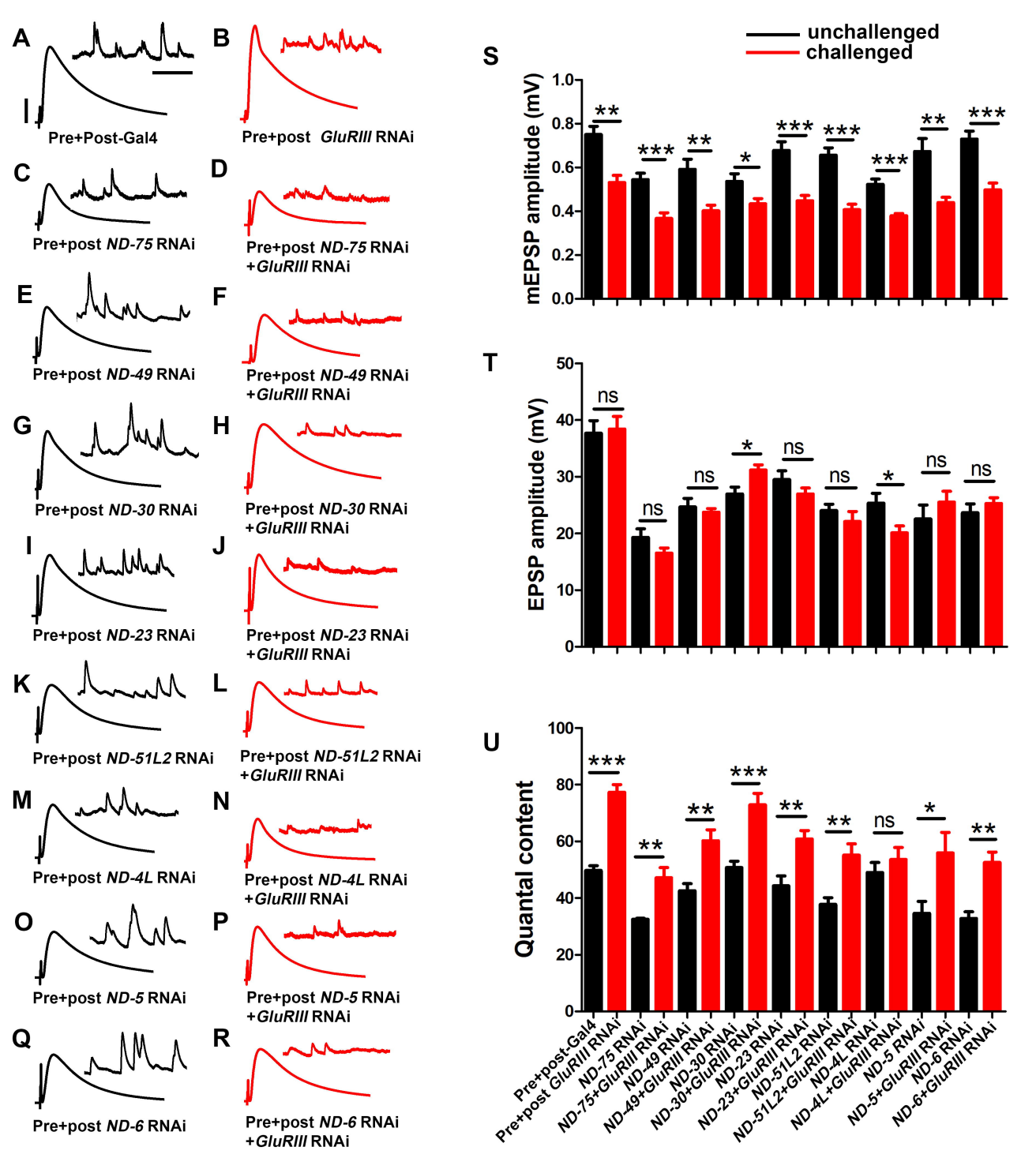
A
Pre+Post-Gal4
B
Pre+post GluRIII RNAi
C
Pre+post ND-75 RNAi
D
Pre+post ND-75 RNAi
+GluRIII RNAi
E
Pre+post ND-49 RNAi
F
Pre+post ND-49 RNAi
+GluRIII RNAi
G
Pre+post ND-30 RNAi
H
Pre+post ND-30 RNAi
+GluRIII RNAi
I
Pre+post ND-23 RNAi
J
Pre+post ND-23 RNAi
+GluRIII RNAi
K
Pre+post ND-51L2 RNAi
L
Pre+post ND-51L2 RNAi
+GluRIII RNAi
M
Pre+post ND-4L RNAi
N
Pre+post ND-4L RNAi
+GluRIII RNAi
O
Pre+post ND-5 RNAi
P
Pre+post ND-5 RNAi
+GluRIII RNAi
Q
Pre+post ND-6 RNAi
R
Pre+post ND-6 RNAi
+GluRIII RNAi
S
unchallenged
challenged
mEPSP amplitude (mV)
1.0
0.8
0.6
0.4
0.2
0.0
**
***
**
*
***
***
***
**
***
T
EPSP amplitude (mV)
50
40
30
20
10
0
ns
ns
ns
*
ns
ns
*
ns
ns
U
Quantal content
100
80
60
40
20
0
***
**
**
***
**
**
ns
*
**
Pre+post-Gal4
Pre+post GluRIII RNAi
ND-75 RNAi
ND-75+GluRIII RNAi
ND-49 RNAi
ND-49+GluRIII RNAi
ND-30 RNAi
ND-30+GluRIII RNAi
ND-23 RNAi
ND-23+GluRIII RNAi
ND-51L2 RNAi
ND-51L2+GluRIII RNAi
ND-4L RNAi
ND-4L+GluRIII RNAi
ND-5 RNAi
ND-5+GluRIII RNAi
ND-6 RNAi
ND-6+GluRIII RNAi

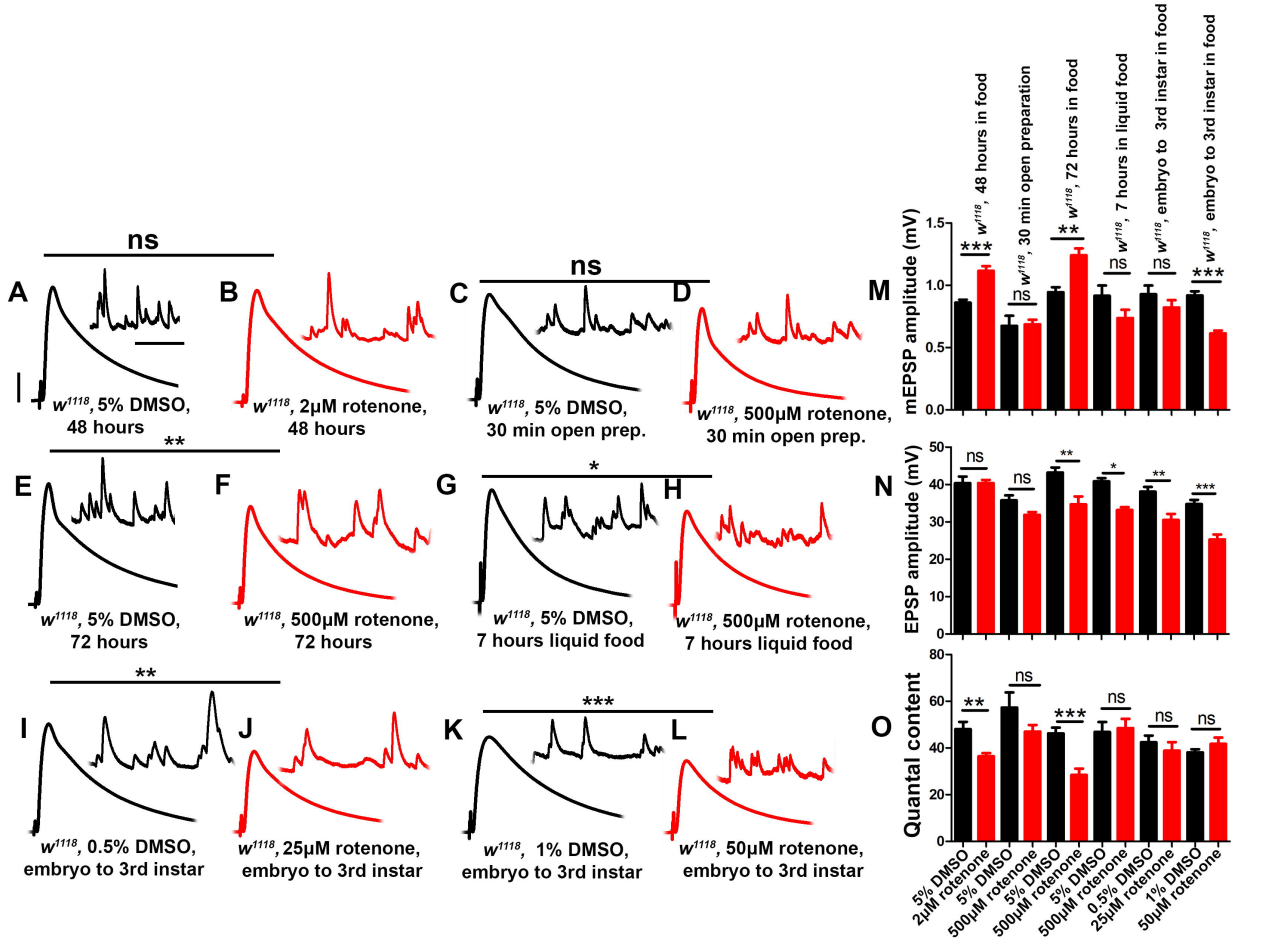
A
B
C
D
E
F
G
H
I
J
K
L
M
N
O
ns
**
*
***
w1118, 5% DMSO, 48 hours
w1118, 2μM rotenone, 48 hours
w1118, 5% DMSO, 30 min open prep.
w1118, 500μM rotenone, 30 min open prep.
w1118, 5% DMSO, 72 hours
w1118, 500μM rotenone, 72 hours
w1118, 5% DMSO, 7 hours liquid food
w1118, 500μM rotenone, 7 hours liquid food
w1118, 0.5% DMSO, embryo to 3rd instar
w1118, 25μM rotenone, embryo to 3rd instar
w1118, 1% DMSO, embryo to 3rd instar
w1118, 50μM rotenone, embryo to 3rd instar
w1118, 48 hours in food
w1118, 30 min open preparation
w1118, 72 hours in food
w1118, 7 hours in liquid food
w1118, embryo to 3rd instar in food
w1118, embryo to 3rd instar in food
mEPSP amplitude (mV)
EPSP amplitude (mV)
Quantal content
5% DMSO
2μM rotenone
5% DMSO
500μM rotenone
5% DMSO
500μM rotenone
5% DMSO
500μM rotenone
0.5% DMSO
25μM rotenone
1% DMSO
50μM rotenone

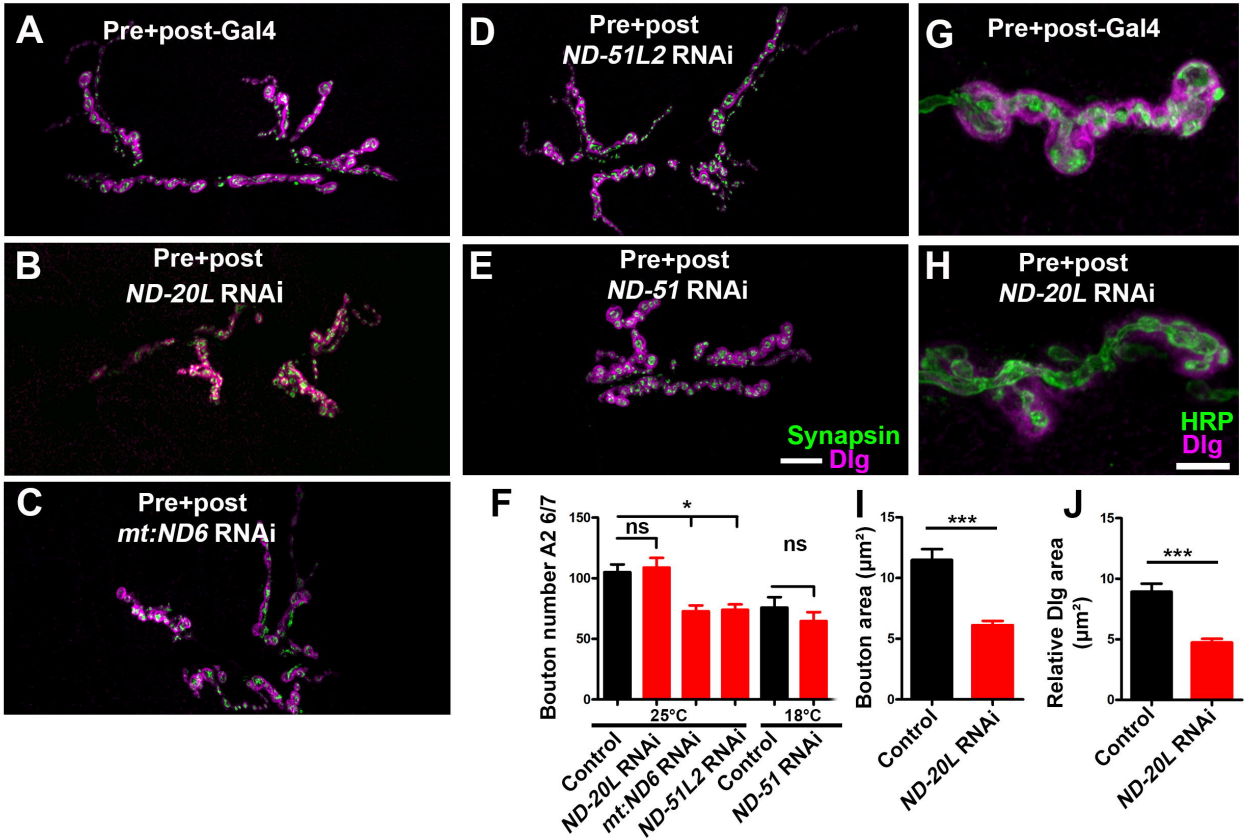
A
Pre+post-Gal4
B
Pre+post
ND-20L RNAi
C
Pre+post
mt:ND6 RNAi
D
Pre+post
ND-51L2 RNAi
E
Pre+post
ND-51 RNAi
Synapsin
Dlg
G
Pre+post-Gal4
H
Pre+post
ND-20L RNAi
HRP
Dlg
F
Bouton number A2 6/7
150
100
50
0
ns
*
ns
25°C
18°C
Control
ND-20L RNAi
mt:ND6 RNAi
ND-51L2 RNAi
Control
ND-51 RNAi
I
Bouton area (µm²)
15
10
5
0
***
Control
ND-20L RNAi
J
Relative Dlg area (µm²)
15
10
5
0
***
Control
ND-20L RNAi